ELSEVIER

Seminars in
RADIATION
ONCOLOGY

Imaging Metabolic Processes to Predict Radiation Responses

Sarwat Naz, PhD,* Shun Kishimoto, MD, MHSc,* James B. Mitchell, PhD,* and Murali C. Krishna, PhD*

The aberrant vasculature in the tumor microenvironment creates hypoxic zones, poor perfusion, and high interstitial fluid pressure. Also, the tumor cell metabolic phenotype utilizes the aerobic glycolytic pathways for energy source and generation of cell mass. These physiologic and metabolic phenotypes in solid tumors are amenable for molecular imaging techniques to extract imaging biomarkers such as pO_2 and enzyme kinetics reflecting glycolysis. The imaging biomarkers have value in diagnostic and prognostic purposes. Additionally, they can be used to guide choices for tailored treatment regimens. Electron paramagnetic resonance imaging for pO_2 imaging and ^{13}C magnetic resonance imaging with hyperpolarized ^{13}C probes such as ^{13}C-labeled pyruvate have shown significant potential in characterizing the tumor microenvironment physiologically and metabolically.
Semin Radiat Oncol 29:81–89

Introduction

Malignant cells have altered energetic demands compared to normal cells to support metabolic activities which generate building blocks for further growth in anabolic processes.[1,2] Whether these altered metabolic pathways are causative or consequential is still a topic for further research. Efforts in unraveling these unknowns can help better understand the basic cell biology of tumors and develop targets for which drug discovery efforts can be directed. The essential growth pressure in cancer cells is dependent on oncogenic reprogramming to generate building blocks in bioenergetic pathways for anabolic growth.[3,4] Such metabolic reprogramming, which is required for tumor growth, can be exploited to target with drugs which can inhibit key bioenergetic pathways in such processes.[5]

In addition to the metabolic differences between tumor cells and normal cells, the physiology of tumors is also significantly different compared to normal tissue in terms of microcirculation features. Tumors grow to a size of 2-3 mm^3 relying on passive supply of nutrients and oxygen. To grow beyond this size, tumors activate angiogenesis pathways to develop new vascular networks.[6] The tumor angiogenesis is not tightly regulated resulting in the development of architecturally and functionally abnormal vessel network.[7] This network is neither as efficient nor well organized in delivering oxygen and nutrients. A major consequence of this situation is the development of diffusion limited chronic hypoxia and acute hypoxia in addition to acidotic conditions.[8] Such microenvironmental conditions in which tumor cells exist allow the acquisition of aggressive phenotype, promote metastasis, and development of resistance to radiation and chemotherapeutic drugs. Such harsh microenvironmental features unique to tumors are characterized by low pO_2, low pH, high interstitial fluid pressure, and leaky vasculature. These unique features offer imaging techniques the capability to obtain biomarkers which can quantitatively characterize such conditions and help in selection and development of appropriate therapies based on information obtained prior to treatment.

Medical imaging is an essential component in the diagnosis and monitoring treatment in various disease conditions including cancer. Most imaging techniques in routine use for diagnostic purposes provide images with excellent anatomic details making it possible to characterize pathologic regions based on morphology and also monitor treatment response by following changes in size. Magnetic resonance imaging (MRI) and computed tomography (CT) are two most common used medical imaging techniques. Treatment response in solid tumors is mostly monitored by measuring volumetric changes after a specified time post treatment. These changes manifest several weeks after the

*Radiation Biology Branch, Center for Cancer Research, National Cancer Institute, Bethesda, MD
Conflict of interest: none.
Address reprint requests to Sarwat Naz, PhD, Radiation Biology Branch, National Cancer Institute, Bldg. 10, Room B3-B69, Bethesda, MD 20892. E-mail: sarwat.naz@nih.gov

https://doi.org/10.1016/j.semradonc.2018.10.004
1053-4296/

initiation of treatment. Thus, prognostic information from such techniques is available very late in the course of treatment. If a particular treatment is ineffective, such information is not available at early stages of treatment to make adjustments/changes to other treatment modalities. Molecular, metabolic, and biochemical changes in tumors in response to treatment are known to manifest as early as 12-36 hours after the treatment has been initiated. Further, profiling the tumor on the basis of biochemical/physiological properties provides an added advantage of choosing appropriate treatment modalities for optimal responses. Molecular imaging, a recently emerging field in preclinical research and in clinical practice has the potential to provide capabilities to characterize the tumor microenvironment based on a metabolic and physiological basis.

One of the features of the tumor microenvironment is hypoxia, which results from aberrant tumor vasculature resulting in inadequate delivery of oxygen and nutrients.[9] The consequences arising from such a situation are chronic and/or transient hypoxia where the tumor pO_2 values can be < 10 mm Hg.[10] Tumor hypoxia has been associated with poor treatment outcome for radiotherapy and even some chemotherapy drugs.[11,12] More recently, tumor hypoxia is thought to be a major factor underlying immunosuppression and resistance to immunotherapy in solid tumors[13-16]. Molecular imaging techniques which can obtain information pertaining to tumor pO_2 and also probe the spatio-temporal heterogeneity of tumor oxygenation will be of significant clinical utility in radiotherapy since such information can be integrated in radiation treatment planning to deliver higher doses to subregions of the tumor exhibiting hypoxia. Most techniques assessing tumor hypoxia are invasive, qualitative, or both. Optimal oxygen imaging techniques should be non-invasive, quantitative, and be capable of serial imaging. It should also be possible to have sufficient temporal resolution to probe dynamics of tumor oxygenation to distinguish chronic versus acute hypoxic regions.

Metabolic imaging of cancer has also become a major area of interest in the recent years. Tumors often times reprogram their metabolic profile in many cases to aerobic glycolysis for transformation and progression. Currently, several metabolic targets are being evaluated in drug development research to preferentially target these pathways and starve the tumors of energy sources. In this context, metabolic imaging is relevant in pharmacodynamics validation of drug actions. Metabolic imaging is also becoming useful to develop diagnostic and prognostic information. Endogenous substrates of cellular energetic processes which are enriched with ^{13}C at suitable sites in metabolic substrates can be hyperpolarized to bridge the sensitivity gap necessary for biochemical imaging using ^{13}C MRI. Very recently, this technique was implemented in the clinic after several years of preclinical research experience.

In this review, preclinical research on molecular imaging of tumor xenografts in mice probing for changes in physiological and biochemical features will be presented to highlight the potential of such information in guiding and monitoring responses to treatment.

Imaging Tumor Oxygenation Using Electron Paramagnetic Resonance

There are several methods to profile tumor oxygenation. Polarographic electrodes such as Eppendorf probes provide quantitative information on tumor pO_2 using invasive procedures.[17] Imaging methods such as Positron Emission Tomography (PET) and Blood Oxygenation Level Dependent (BOLD) Magnetic Resonance Imaging (MRI) provide noninvasive assessment of tumor oxygenation qualitatively. Electron paramagnetic resonance (EPR) imaging is unique in its capability in providing quantitative maps of tumor pO_2 noninvasively. EPR spectroscopy is similar to NMR spectroscopy and detects paramagnetic species with unpaired electrons. Nuclear Magnetic Resonance (NMR) spectroscopy using magnetic field gradients evolved into MRI. The abundant water protons in soft tissue (~70 M) and the strongest magnetic moment of ^{1}H among all nuclei and simple NMR spectrum enable the feasibility of MRI in live objects. EPR spectroscopy detects paramagnetic species such as free radicals and transition metal complexes. Free radical EPR spectra can be detected at physiological temperatures unlike with transition metal complexes. However, unlike MRI, the vanishingly low concentrations of endogenous free radicals (<nM) and their chemical instability made EPR imaging in live objects nonfeasible. With the recent development of trityl radicals (eg, Ox063) which are stable organic free radicals with simple EPR spectrum, pharmacologic half-life ~15 mins and minimal to no toxicity at the doses needed for imaging have made in vivo EPR imaging feasible.[18,19] Ox063 is now most widely used for in vivo EPR applications. The collisional interaction between Ox063 and paramagnetic molecular oxygen results in shortening of T2 of the radical and broadening of its EPR spectral line width. The extent of line broadening is linearly proportional to oxygen concentration. By extracting the line width of Ox063 after intravenous infusion and generating spatial images using magnetic field gradients, it is possible to experimentally obtain line widths from each voxel from which pO_2 maps can be generated with appropriate calibrations.

Anatomically coregistered maps and steady state levels of metabolites in different regions of the tumor with different levels of pO_2 were studied using EPR and MRI.[20] Figure 1A shows the anatomic image of the SCCVII tumor-bearing leg and normal leg from a C3H mouse obtained using a T2-weighted MRI scan, whereas the right panel of Figure 1B shows the corresponding pO_2 image from the same mouse after administration of Ox063. The normal leg displayed pO_2 corresponding to normoxia with minimal heterogeneity. On the other hand, the tumor showed significantly hypoxic regions along with normoxic regions. This capability of generating anatomically coregistered quantitative maps of tumor pO_2 using EPR with a biocompatible infusible paramagnetic tracer makes this technique unique among the pO_2 imaging methods. Volume selective ^{1}H magnetic resonance spectroscopy was carried out on the same tumor where 3 voxels (indicated by the 3 green squares in Fig. 1A) were selected based on the pO_2 information from EPR image (Fig. 1C). The ^{1}H spectra show the metabolites total choline (tCho),

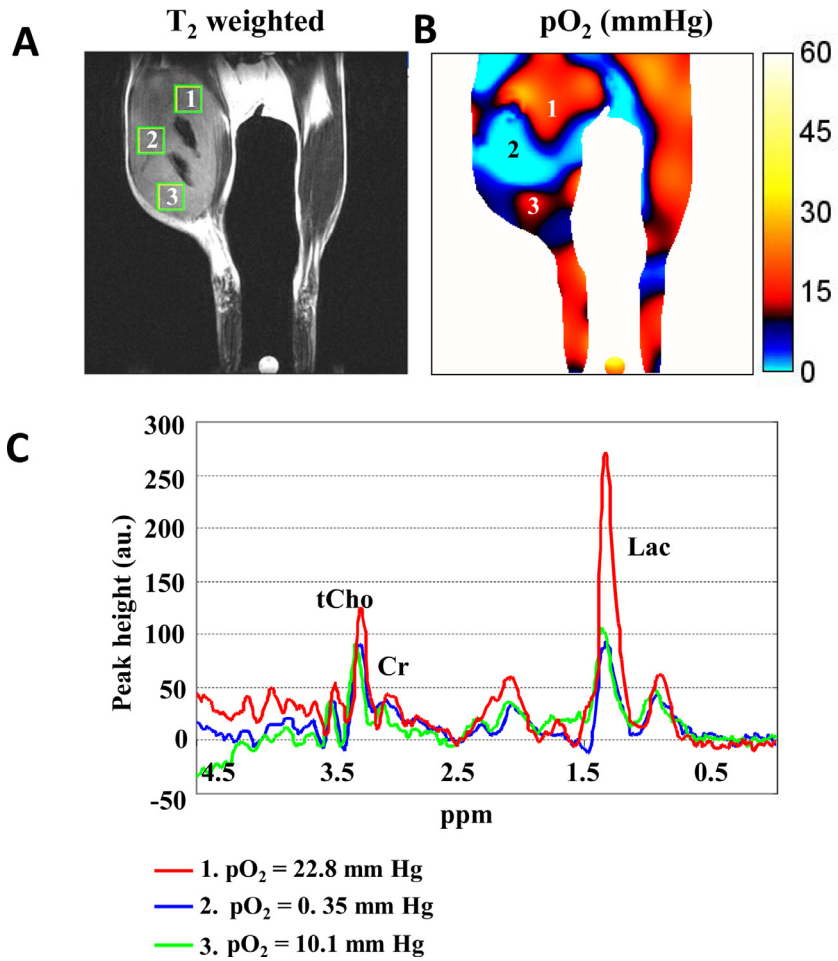

Figure 1 Images of pO_2 distribution and metabolite levels in tumors. (A) T2-weighted anatomical MRI image of SCC tumor-bearing mouse and ROI locations for MRS. (B) EPRI pO_2 map of the same animal and the corresponding ROIs chosen for MRS. Numbers 1-3 in A-B correspond with numbers 1-3 in C. (C) Representative MRS spectra obtained from 3 different tumor regions selected with different pO_2 Cr, creatine; Lac, lactate; tCho, total choline. (Adapted from Matsumoto et al.[20])

creatine (Cr), and lactate (Lac) to determine the steady state levels of metabolites at different levels of pO_2 in the tumor. The results indicated that even a well-oxygenated region of the tumor can have high lactate levels suggesting onset of an efficient aerobic glycolysis pathway (Warburg Effect).

To examine the extent of hypoxia (pO_2 < 10 mm Hg) as a function of tumor size, EPR imaging studies were carried out in SCCVII tumors in C3H mice between day 3 and day 14 after implantation.[21] Figure 2 shows that a significant increase in tumor hypoxia is observed as the tumor size increases, consistent with histologic studies showing that with increasing size, tumors often have inadequate perfusion and oxygenation.

EPR imaging studies on 2 different types of tumors, SCCVII in C3H mice and HT29 in SCID mice were conducted to examine patterns of tumor oxygenation.[22] Figure 3A shows the anatomic image and pO_2 of SCCVII tumor in C3H mice and HT29 tumor in SCID mice. Both tumors showed a significant extent of hypoxia with the median pO_2 values lower in the SCCVII (10.9 mm Hg) than HT29 tumors (14.5 mm Hg) (Fig. 3B). The HF10 (hypoxic fraction; pO_2 < 10 mm Hg) and HF15.2 (hypoxic fraction; pO_2 < 15.2 mm Hg) values in these 2 tumors showed significant differences (Fig. 3C). The SCCVII tumor at 980 mm^3 size had HF15.2 and HF10 of ~80% and 50%, respectively, while these values for HT29 tumors were 53% and 25%, respectively, suggesting that the HT29 tumor is less hypoxic than the SCCVII tumor. Since tumors are known to have regions of chronic hypoxia as well as acute or transient hypoxia, EPR imaging studies were applied to probe the dynamics of tumor pO_2 in the SCCVII and HT29 tumors.[23] Figure 4A shows the anatomic MRI scan with regions of interest (ROI) marked in various parts of the SCCVII tumor and the corresponding pO_2 maps taken every three minutes (Fig. 4B). The pO_2 values from each of the 4 regions were plotted and shown in Figure 4C. The peripheral region of the tumor (ROI-1) displayed remarkable fluctuations in pO_2 from 35 mm Hg—nearly 0 mm Hg within a few minutes and recovered back. ROI-2 which was also a peripheral region displayed similar profile. This pattern has been attributed to acute or cycling hypoxic regions, while ROI 3 was stable at ~10 mm Hg. However, ROI-4 was stable and nearly completely hypoxic, typical of

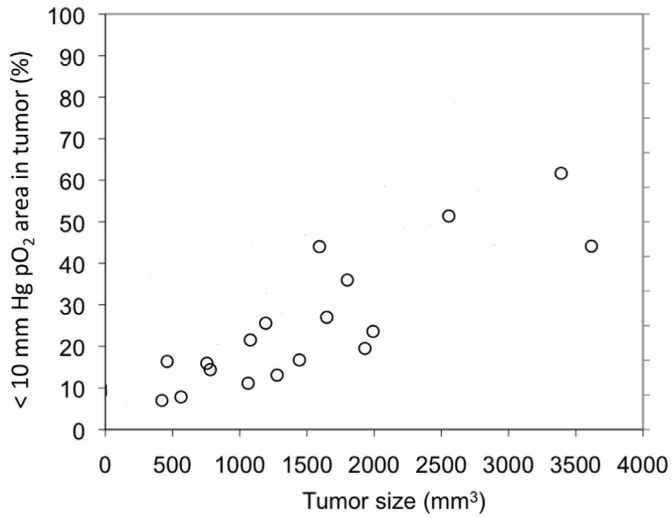

Figure 2 Relationship between tumor pO_2 and tumor size. (Hyodo et al.[21])

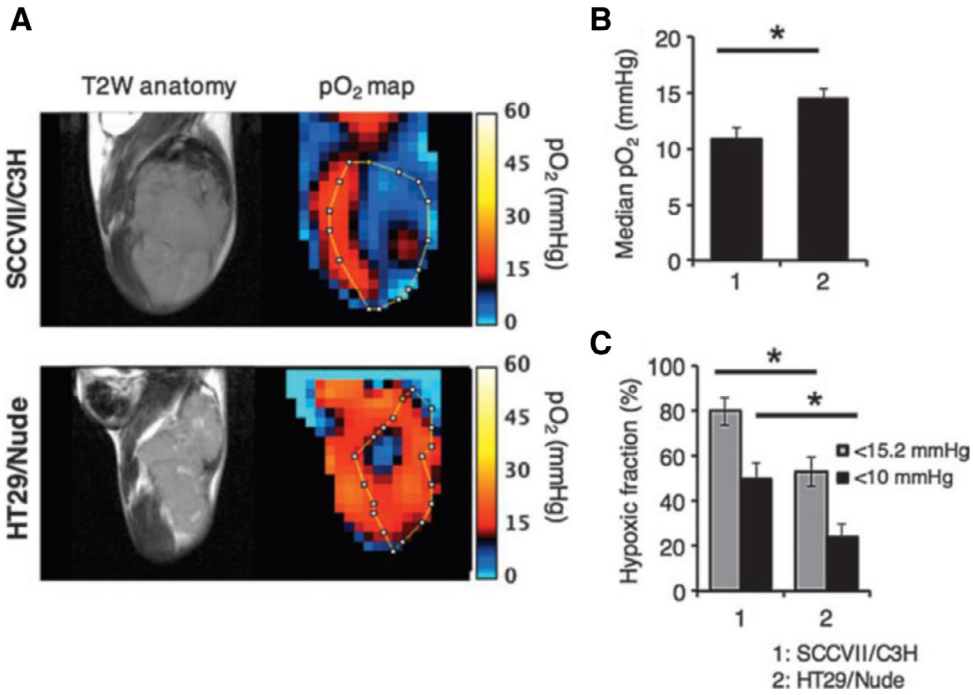

Figure 3 EPRI/MRI in SCCVII (n = 3) and HT29 tumors (n = 4). (A-C) Noninvasive monitoring and quantification of tumor median pO_2 by EPR oximetry. (A) T2-weighted anatomical images and pO_2 maps of SCCVII or HT29 (*800 mm^3). (B, C) Changes in median pO_2 (B) and proportional hypoxic regions (C). Each value was measured across three 2-mm slices. *$P < 0.05$. EPRI, electron paramagnetic resonance imaging; MRI, magnetic resonance imaging. (Takakusagi et al.[24])

diffusion limited hypoxia, or chronic hypoxia. Similar studies on HT29 tumors showed similar trends though the magnitude of fluctuations in the cycling hypoxic regions was significantly lower than in SCCVII tumors (Figure 4D-,F).

With the assessment of the hypoxia features in these 2 tumors in terms of median pO_2, hypoxic fractions, and the dynamics of tumor pO_2, we further examined the predictive potential of these 2 tumors with radiotherapy and hypoxia-activated prodrug therapy (HAP).[24] Groups of mice with SCCVII tumors and HT29 tumors were followed for survival receiving no treatment (control), monotherapy with radiation (XRT), HAP (eg, TH-302) or combination of XRT + HAP (Fig. 5). At 50% survival, the results show that the more hypoxic SCCVII tumor minimally responded to XRT or TH-302, while a significant benefit was realized with the combination of XRT + TH-302 suggesting that even with hypoxia, normoxic regions are also present which responded to XRT in the

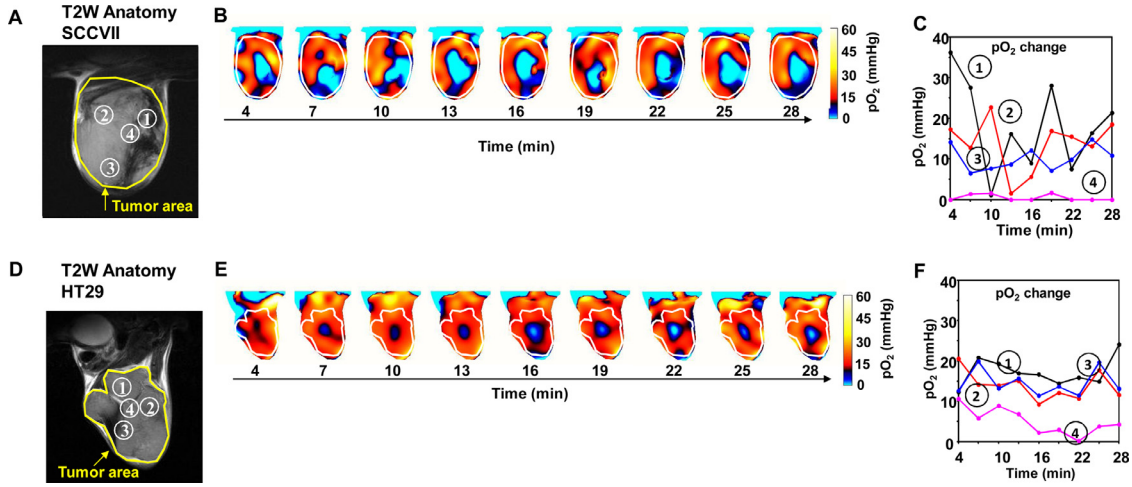

Figure 4 Noninvasive imaging of fluctuating pO_2 in SCCVII tumors and HT29 tumors using EPRI. (A) T2-weighted anatomical image of a representative SCCVII (A) and HT29 tumor-bearing mouse (D) and the corresponding pO_2 maps (B and E) as a function of time. Time increased from left to right from 4 to 28 min. Large yellow line, tumor region. Four ROIs indicated by small white line were chosen for tracing fluctuations of pO_2. The values of pO_2 and the tracer level in each ROI region described in A and D were quantified and plotted as a function of time (C and F). (Adapted from Yasui et al.[23])

combination regimen (Fig. 5A). While the HT-29 tumors on the other hand treated with TH-302 had no benefit in survival, XRT alone showed modest benefit in terms of survival. At 50% survival, XRT alone resulted in 7 days extension compared to control or TH-302 treatment alone suggesting that this tumor physiology, as determined by EPR, had better perfusion and oxygenation. However, the XRT + TH-302 combination in HT29 tumor showed significant enhancement in survival (Fig. 5B).

With these initial studies showing promise of EPR-based pO_2 assessment in providing useful a priori information related to tumor pO_2, a systematic study on 3 different pancreatic ductal adenocarcinoma (PDAC) tumors was studied in mice.[25] The 3 pancreatic cancer cell lines Su86.86, MiaPaca-2, and Hs766t were profiled in vitro using the SeaHorse extracellular flux analyzer for oxygen consumption and aerobic glycolysis. The studies showed that the aerobic glycolysis efficiency of these cells in vitro followed the pattern Hs766t > MiaPaca-2 > Su86.86. In vivo EPR imaging studies were carried out to examine if such differences were exhibited in vivo. The anatomic images and the pO_2 images of these 3 tumor xenografts are shown in Figure 6A and B. The Hs766t tumor had a significant hypoxic fraction, which was greater than the MiaPaca-2 and Su86.86 tumor. The median pO_2 values followed Su86.86 > MiaPaca-2 > Hs766t (Fig. 6C), and the HF10 values followed the pattern Hs766t > MiaPAca-2 > Su86.86 (Fig. 6D). Such information will be useful in testing the value of these imaging biomarkers in planning treatment and evaluating response to treatment. Such information if put in context with molecular

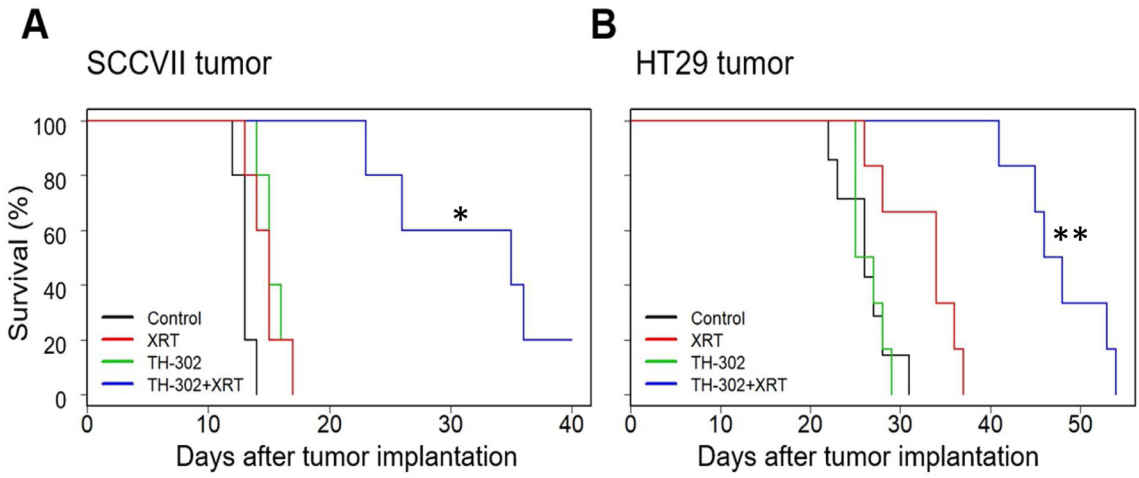

Figure 5 Kaplan-Meier Survival Analysis. (A, B) Kaplan-Meier plot of SCCVII/C3H mice (A) and HT29/nude mice (B) after 5 times of treatment with TH-302 and/or XRT (3 Gy) on SCCVII tumor-bearing C3H/HeN mice (A) and HT29 tumor-bearing athymic nude mice (B). Mice were sacrificed when the tumor volume reached 2000 mm^3. Data are mean ± SE of 5 (A) or 7 (B) mice. $*P < 0.05$, $**P < 0.001$. XRT, radiotherapy. (Adapted from Takakusagi et al.[24])

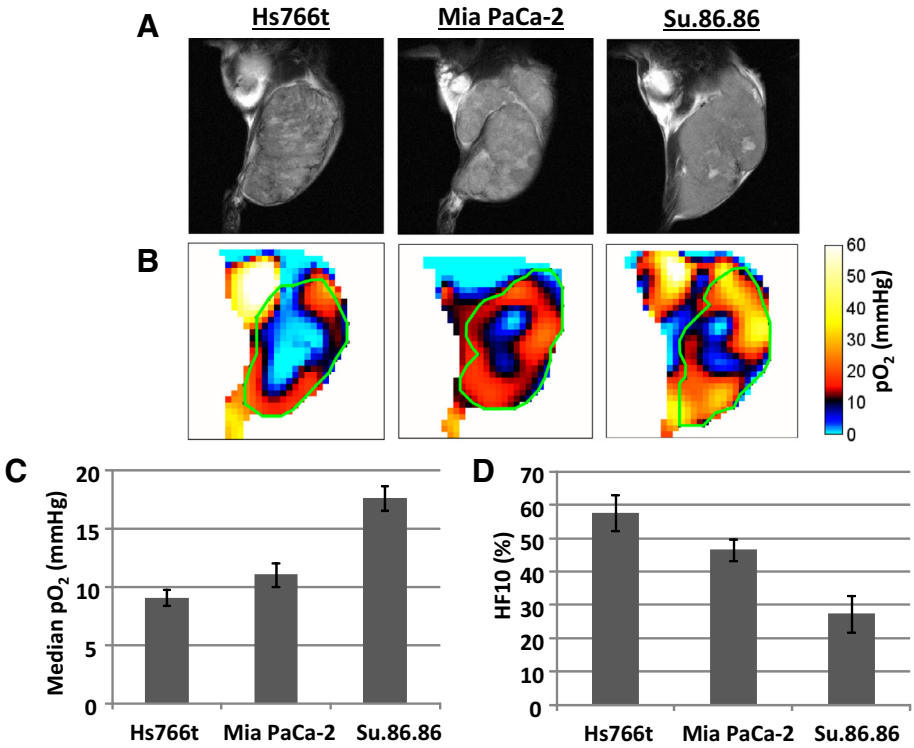

Figure 6 EPR oxygen imaging of 3 PDAC xenografts. (A) Anatomic T2-weighted MR images of Hs766t, MiaPaCa2, and Su.86.68 tumors. (B) Three-dimensional oxygen imaging of the PDAC tumors obtained by EPR imaging. (C, D) Median pO_2 (D) and hypoxic fraction with less than <10 mm Hg pO_2 (E) of the 3 PDCA tumors. Quantitative oxygen imaging revealed that Hs766t is the most hypoxic, and Su.86.86 is the most oxygenated tumor of the 3 PDAC tumors. Data are presented as mean ± SD of 5 tumors for each cell line. (Adapted from Matsumoto et al.[25])

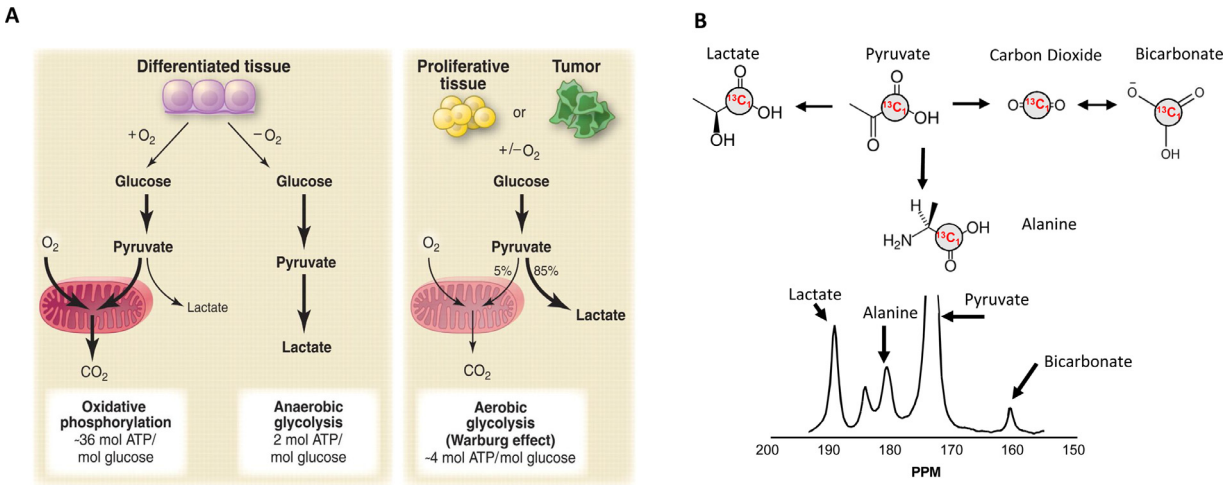

Figure 7 (A) Differences between oxidative phosphorylation, anaerobic glycolysis, and aerobic glycolysis (Warburg effect). In the presence of oxygen, nonproliferating tissues first metabolize glucose to pyruvate via glycolysis and then completely oxidize most of that pyruvate in the mitochondria to CO_2 during the process of oxidative phosphorylation. In tumor cells, even when oxygen is available, glucose is metabolized through aerobic glycolytic pathway generating lactate. (Adapted from Vander Heiden et al.[4] with permission) (B) Schematic representation of various metabolic pathways 1-^{13}C pyruvate participates in and the corresponding NMR peaks.

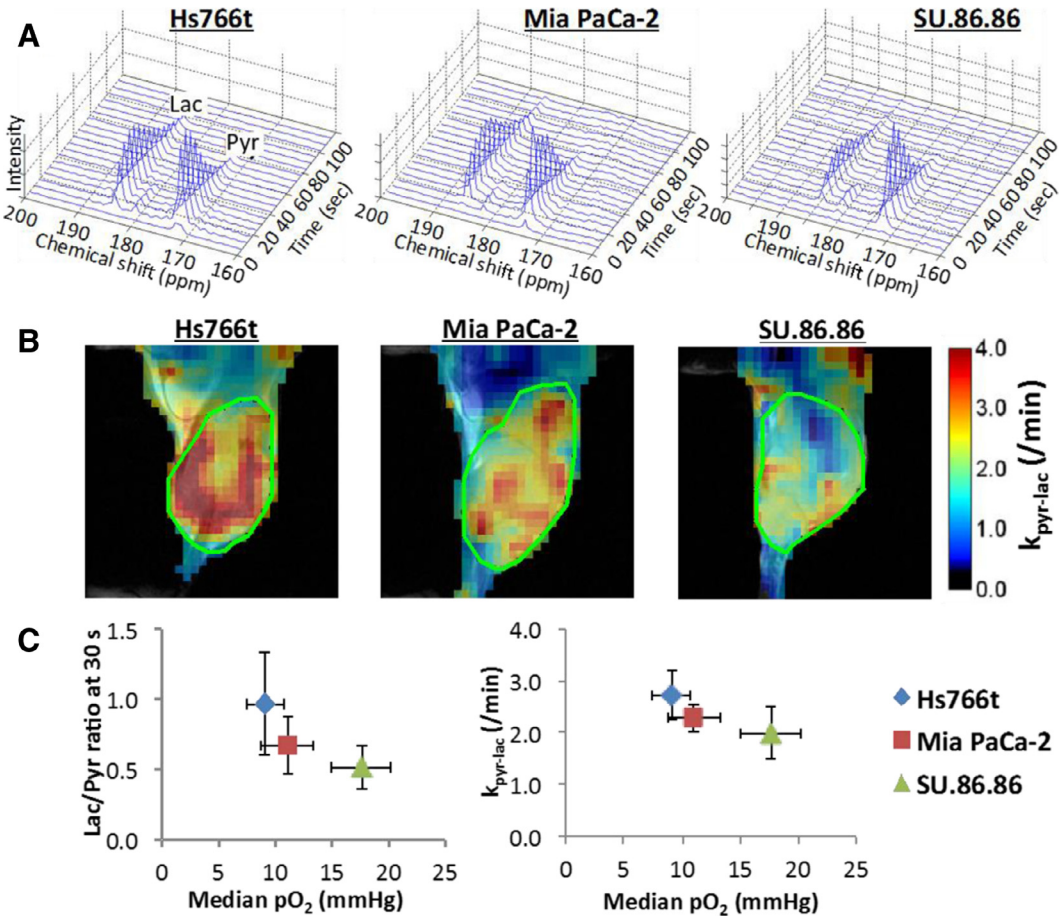

Figure 8 MRI of hyperpolarized ^{13}C pyruvate metabolism in 3 PDAC xenografts. (A) Representative dynamic ^{13}C NMR spectra of a tumor voxel from 3 PDAC tumors. (B) Kinetic constant maps of pyruvate-to-lactate conversion rate constants ($k_{pyr/lac}$), that is, LDH activity, calculated from serial spectroscopic ^{13}C MR images obtained every 6 seconds after hyperpolarized ^{13}C pyruvate injection. (C) Correlation between lactate/pyruvate ratio (left) at 30 seconds after pyruvate injection or pyruvate-to-lactate conversion rate (right) from hyperpolarized ^{13}C MRI (left) and median tumor pO_2 from EPR imaging in 3 pancreatic tumor xenografts. Data are presented as mean ± SD of 6 tumors for each cell line. (From Matsumoto et al.[25])

imaging biomarkers related to biochemical or metabolic profile may provide a more comprehensive assessment of the tumor microenvironment and the inter-relationship between the tumor physiology and metabolism.

Molecular Imaging of Tumor Metabolic Profile With ^{13}C MRI With Hyperpolarized ^{13}C Pyruvate

MRI using tissue water (^{1}H) is feasible because of the abundance of water protons in soft tissue (~70 M) and the strong signals emanating from ^{1}H. Imaging organic metabolites using ^{1}H magnetic resonance spectroscopy is possible using special imaging sequences to determine levels of metabolites such as total choline, lactate, and so on. However, though useful, these levels reflect a steady state condition but do not provide dynamic flux levels produced in biochemical pathways. Dynamic ^{13}C MRI in principle can provide such information. However, approximately 4 orders of magnitude lower sensitivity of ^{13}C MRI of endogenous metabolites compared to ^{1}H MRI of tissue water protons have made such studies not practical in live objects. With the recent discovery of hyperpolarization techniques using dissolution dynamic nuclear polarization, it has been possible to realize a 4-order in magnitude enhancement in ^{13}C MRI. With this approach, a ^{13}C-labeled energy fuel such as glucose, pyruvate, and so on can be hyperpolarized, injected, and the kinetics of their conversion to various metabolites can be monitored. The polarization, relaxation properties, and so on have been reviewed in detail elsewhere.[26] With this capability, ^{13}C MRI can be used to biochemically profile the metabolic differences between normal tissue and malignant tissue. Figure 7A shows the metabolic differences between normal tissue and cancer. Glucose is taken up and metabolized using the citric acid cycle in the mitochondria to generate ATP in the presence of oxygen, a process referred to as oxidative phosphorylation.[4] Only when there is no oxygen available, glucose is metabolized anaerobically to generate ATP. In malignant cells in vitro and in vivo, even in the presence of oxygen, glucose gets metabolized through the

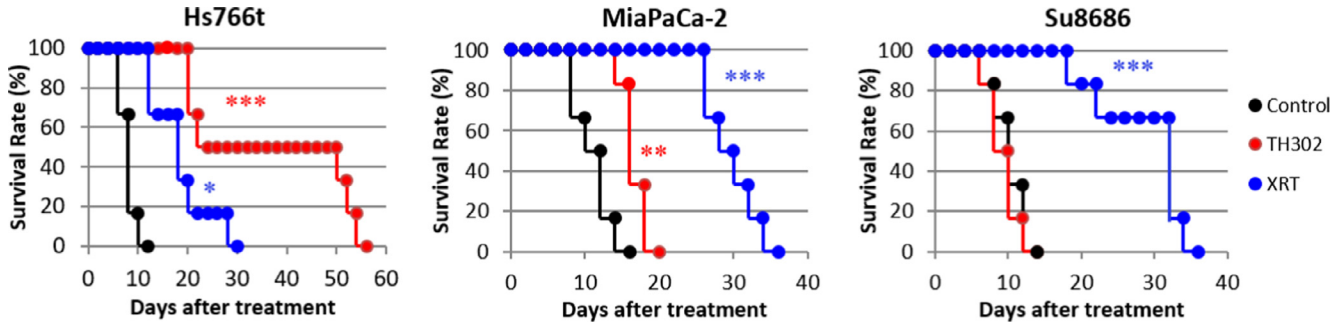

Figure 9 Response of 3 pancreatic tumors to cancer treatments. Mice bearing 1 of 3 PDAC tumors were treated with either gemcitabine (bolus 125 mg/kg), fractionated X-radiation (XRT; 3 Gy × 5 days), or hypoxia-activated prodrug TH-302 (80 mg/kg daily × 5 days). "Survival" was defined as tumor volume increasing by <2.5-fold from the original size. MiaPaCa2 and Su.86.86 tumors responded best to radiotherapy, whereas TH-302 produced the best survival rate in Hs766t tumors. See Table 1 for statistical results on treatment benefit. Each treatment group was compared to control group by log-rank test. *$P > 0.05$, **$P > 0.01$, ***$P > 0.001$. (From Matsumoto et al.[25])

aerobic glycolysis pathway, also known as the Warburg phenotype. It is possible to image these metabolic differences using hyperpolarized ^{13}C-labeled pyruvate. Pyruvate is a downstream metabolite of glucose metabolism. It enters the citric acid cycle for energy production through oxidative phosphorylation. Figure 7B shows the various metabolic pathways where pyruvate is involved in and the corresponding chemical shifts in the NMR spectrum. It enters the citric acid cycle for energy production through oxidative phosphorylation. Alternately, it can be utilized in aerobic glycolysis generating lactate, typically in tumors. 1-^{13}C-labeled pyruvate is one of the most favorable molecules amenable for hyperpolarization and has been used extensively in preclinical models and in humans.

Tumor metabolic profile of the 3 PDAC tumor xenografts Hs766t, MiaPAca-2, and Su86.86 were studied using ^{13}C MRI after injecting hyperpolarized pyruvate and monitoring the kinetics of conversion of pyruvate to lactate.[25] Figure 8A shows the volume selective ^{13}C spectra taken from the 3 tumor xenografts indicating that the Hs766t tumor was most efficient in generating lactate compared to MiaPaca-2 and Su86.86. The kinetics of pyruvate to lactate followed the order Hs766t > MiaPAca-2 > Su86.86. Figure 8B shows the corresponding images of the kinetics of glycolysis which provide a spatial assessment of the Warburg phenotype. The images show that the Hs766t tumor had extensive regions of glycolysis compared to the Su86.86 tumor, whereas the MiaPaca-2 tumors exhibited intermediate behavior. A comparison of tumor hypoxia with the glycolytic kinetics was also done and the data are shown in Figure 8C. An inverse relationship between tumor pO_2 and glycolytic rate was noticed. These results support the notion that the rate of glycolysis can serve as a surrogate for tumor hypoxia. This is an important finding as ^{13}C MRI with pyruvate is now approved for pilot clinical trials. We are hopeful that these early clinical trials may also provide information pertaining to tumor hypoxia.

Further, to examine the utility of these biomarkers to help treatment selection, groups of mice bearing these 3 tumors were treated with XRT alone or the HAP (TH-302) alone and survival compared to untreated controls. As predicted by the 2 imaging modalities, the Hs766t tumor showed a modest response to radiation compared to TH-302, while the SU86.86 tumor showed significant response to radiation while no response to TH-302. The MiaPAca-2 tumor showed modest response to TH-302 compared to XRT (Fig. 9). Table 1 summarizes the treatment benefit (growth delay) in these 3 groups of mice. To the extent that these murine model studies apply to humans, these preclinical studies clearly show that molecular imaging biomarkers can provide pretreatment assessment of tumor physiology and metabolism to aid in the choice of treatment.

Table 1 Treatment Benefit (Growth Delay) of Monotherapy and Combination Therapy

	Hs766t	MiaPaca-2	Su.86.86
TH-302	25.0 ± 7.7	6.7 ± 0.7	0.7 ± 0.6
XRT	6.3 ± 2.7	16.7 ± 1.6	18.0 ± 2.7
XRT + TH-302	>50.7 ± 0.7	>37.7 ± 3.1	22.3 ± 0.7

Treatment benefit (days) = (days to 2.5 times) − (nontreat). " > " Represents the group include mice that survived past 60-day end point.

Summary

Molecular imaging techniques have become powerful tools in characterizing the tumor microenvironment. Using such techniques to guide treatment selection will hopefully provide better clinical outcomes with chemotherapy, chemoradiation, hypoxic cytotoxins, and perhaps immunotherapy.

References

1. Hanahan D, Weinberg RA. Hallmarks of cancer: The next generation. Cell 144:646-674, 2011
2. DeBerardinis RJ, Thompson CB. Cellular metabolism and disease: What do metabolic outliers teach us. Cell 148:1132-1144, 2012
3. Vander Heiden MG, DeBerardinis RJ. Understanding the intersections between metabolism and cancer biology. Cell 168:657-669, 2017

4. Vander Heiden MG, Cantley LC, Thompson CB. Understanding the Warburg effect: The metabolic requirements of cell proliferation. Science 324:1029-1033, 2009
5. Deberardinis RJ, Sayed N, Ditsworth D, et al: Brick by brick: Metabolism and tumor cell growth. Curr Opin Genet Dev 18:54-61, 2008
6. Folkman J. Tumor angiogenesis: Therapeutic implications. N Engl J Med 285:1182-1186, 1971
7. Jain RK, Carmeliet PF. Vessels of death or life. Sci Am 285:38-45, 2001
8. Dewhirst MW. Relationships between cycling hypoxia, HIF-1, angiogenesis and oxidative stress. Radiat Res 172:653-665, 2009
9. Brown JM. Tumor hypoxia in cancer therapy. Methods Enzymol 435:297-321, 2007
10. Chaplin DJ, Durand RE, Olive PL. Acute hypoxia in tumors: Implications for modifiers of radiation effects. Int J Radiat Oncol Biol Phys 12:1279-1282, 1986
11. Hockel M, Schlenger K, Aral B, et al: Association between tumor hypoxia and malignant progression in advanced cancer of the uterine cervix. Cancer Res 56:4509-4515, 1996
12. Brizel DM, Sibley GS, Prosnitz LR, et al: Tumor hypoxia adversely affects the prognosis of carcinoma of the head and neck. Int J Radiat Oncol Biol Phys 38:285-289, 1997
13. Palazón A, Aragonés J, Morales-Kastresana A, et al: Molecular pathways: Hypoxia response in immune cells fighting or promoting cancer. Clin Cancer Res 18:1207-1213, 2012
14. Barsoum IB, Smallwood CA, Siemens DR, et al: A mechanism of hypoxia-mediated escape from adaptive immunity in cancer cells. Cancer Res 74:665-674, 2014
15. Damgaci S, Ibrahim-Hashim A, Enriquez-Navas PM, et al: Hypoxia and acidosis: Immune suppressors and therapeutic targets. Immunology 154:354-362, 2018
16. Ngwa W, Irabor OC, Schoenfeld JD, et al: Using immunotherapy to boost the abscopal effect. Nat Rev Cancer 18:313-322, 2018
17. Matsuo M, Matsumoto S, Mitchell JB, et al: Magnetic resonance imaging of the tumor microenvironment in radiotherapy: Perfusion, hypoxia, and metabolism. Semin Radiat Oncol 24:210-217, 2014
18. Matsumoto K, Hyodo F, Matsumoto A, et al: High-resolution mapping of tumor redox status by magnetic resonance imaging using nitroxides as redox-sensitive contrast agents. Clin Cancer Res 12:2455-2462, 2006
19. Subramanian S, Yamada K, Irie A, et al: Noninvasive in vivo oximetric imaging by radiofrequency FT EPR. Magn Reson Med 47:1001-1008, 2002
20. Matsumoto S, Hyodo F, Subramanian S, et al: Low-field paramagnetic resonance imaging of tumor oxygenation and glycolytic activity in mice. J Clin Invest 118:1965-1973, 2008
21. Hyodo F, Davis RM, Hyodo E, et al: The relationship between tissue oxygenation and redox status using magnetic resonance imaging. Int J Oncol 41:2103-2108, 2012
22. Takakusagi Y, Matsumoto S, Saito K, et al: Pyruvate induces transient tumor hypoxia by enhancing mitochondrial oxygen consumption and potentiates the anti-tumor effect of a hypoxia-activated prodrug TH-302. PLoS One 9:e107995
23. Yasui H, Matsumoto S, Devasahayam N, et al: Low-field magnetic resonance imaging to visualize chronic and cycling hypoxia in tumor-bearing mice. Cancer Res 70:6427-6436, 2010
24. Takakusagi Y, Kishimoto S, Naz S, et al: Radiotherapy synergizes with the hypoxia-activated prodrug evofosfamide: In vitro and in vivo studies. Antioxid Redox Signal 28:131-140, 2018
25. Matsumoto S, Kishimoto S, Saito K, et al: Metabolic and physiologic imaging biomarkers of the tumor microenvironment predict treatment outcome with radiation or a hypoxia-activated prodrug in mice. Cancer Res 78:3783-3792, 2018
26. Ardenkjaer-Larsen JH, Fridlund B, Gram A, et al: Increase in signal-to-noise ratio of >10,000 times in liquid-state NMR. Proc Natl Acad Sci U S A 100:10158-10163, 2003